https://doi.org/10.37434/tpwj2021.01.03

PREDICTION OF RESIDUAL STRESSES AFTER WELDING OF DUPLEX STEEL TAKING INTO ACCOUNT PHASE TRANSFORMATIONS

O.S. Kostenevych[1] and **JR en**[2]
[1]The Experimental Design and Technological Bureau of the E.O. Paton Electric Welding Institute of the NAS of Ukraine
15 Kazymyr Malevych Str., 03150, Kyiv, Ukraine. E-mail: alenakostenevich@gmail.com
[2]School of Engineering, Liverpool John Moores University
3 Byron Str., United Kingdom. E-mail: x.j.ren@ljmu.ac.uk

The presented study involved mathematical modelling of single pass TIG welding of duplex stainless steel S32205. The temperature fields, the fusion zone and HAZ dimension, the cooling rate fields, residual stresses taking into account kinetics of dissolution of austenite during heating and kinetics of precipitation of austenite during cooling were obtained. The comparative analysis of residual stresses with/without phase transformations showed the difference of residual stresses distribution due to different amounts of austenite and ferrite and due to volumetric changes during phase transformations. 24 Ref, 1 Table, 9 Figures.

K e y w o r d s : duplex stainless steel, TIG welding, phas e transformations, austenite, ferrite, residual stresses

Duplex stainless steels (DSSs) contain approximately equal amounts of austenite (γ) and ferrite (α), which offer many advantages over other single phased stainless steels. DSSs have higher strength than austenitic steels, higher impact value and higher resistance against hydrogen embrittlement than ferritic steels. DSSs with optimum volume fractions of ferrite and austenite also possess a higher resistance against general corrosion, intergranular, pitting, crevice corrosion and stress-corrosion cracking. The application of DSSs covers a broad range of industries such as the oil and gas, petrochemical, chemical industries, energy industry, marine structures, as well as general structures such as architecture, building, construction and mechanical engineering. For most of these applications, the combination of strength and corrosion resistance is a particularly important consideration for the design, manufacturing and structure maintenance. Many of these applications involve welding of similar or dissimilar grades of DSSs with different types of welding [1–5] including tungsten inert gas (TIG) welding.

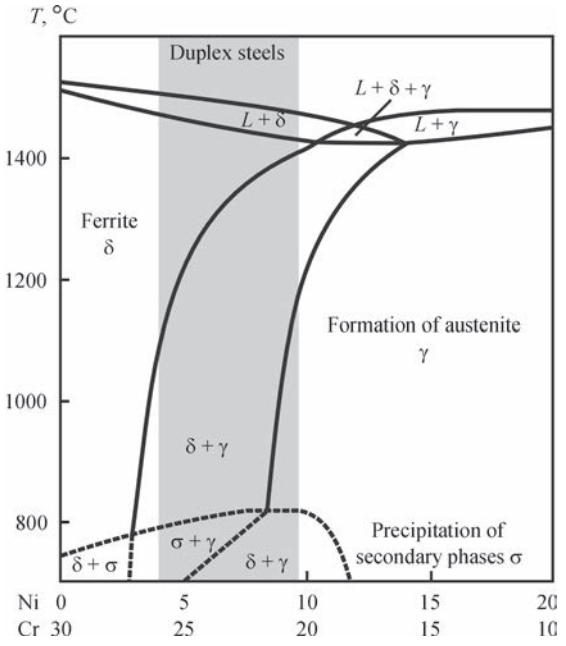

Figure 1. Phase diagram of the triple system Fe–Cr–Ni at 70 % Fe [1, 6, 7]

When welding duplex steels, a general requi rement during welding of DSSs is limitation of the welding heat input. The upper temperature limit of heat input is limited by the formation of intermetallic phases, and the lower — by an acceptable ratio of austenite and ferrite. It is recommended to adhere to a heat input of 0.5–2.5 kJ/mm for steels containing 22 % chromium and 0.2–1.5 kJ/mm for super duplex steels with 25 % chromium [1, 2]. One major focus for welding process design is to retain the good combination of properties, which is sensitive to the chemical composition and microstructure of the fusion and heat-affected zones (HAZ). Particular features governing the structural integrity are the volume fractions of the ferrite and austenite phases, the phase transfor-

O.S. Kostenevych — https://orcid.org/0000-0002-7427-2805, J. Ren — https://orcid.org/0000-0001-6132-1228

Chemical composition for 2205 grade stainless steel [4]

Grade	C	Mn	Si	Cr	Mo	Ni	N	P	S
2205 (S32205)	<0.03	<2.0	<1.0	22.0–23.0	3.0–3.5	4.5–6.5	0.14–0.20	<0.03	<0.02

mation over critical temperature-composition ranges (Figure 1) and residual stresses.

Many recent work have reported on the phase volumes changes in welding DSSs, but systematic works on the effect of microstructural phase transformations on residual stresses are still limited [8–12]. Residual stresses in welding are an important factor influencing both the mechanical strength and the corrosion resistance of DSSs, such an issue needs to be addressed with good accuracy taking into account phase transformations.

This work presents a comparative analysis of the distribution of residual stresses after welding of DSS taking into account microstructural transformations. The main mathematical models, numerical procedures and typical results are introduced. The work is applied in analyzing TIG welding of standard duplex steel S32205, the data includes temperature fields, characteristic cooling rates and microstructure composition. The residual stresses distribution with/without phase transformations is presented and discussed.

Modelling approaches of the temperature fields and phase transformations. In this work, the TIG welding process of standard duplex stainless steel S32205 (Table) taking into account microstructural transformations was simulated and temperature fields, characteristic cooling rates, microstructure composition and residual stresses were obtained. The analysis is focused on single pass TIG welding process without preheating: I = 120 A, U = 10 V, welding speed 1.5 mm/s. The heat input was H = 600 J/mm, which is in the recommended range of 512 < H < 2520 J/mm for welding of duplex steels [2].

The chemical composition of standard duplex steel S32205 is listed in Table. Thermo-physical properties of base material were adapted from literature data [12, 13]. The latent heat of fusion is 300 J/g.

Simulation has been carried out using finite element calculation model (ABAQUS) on a plate of thickness 3 mm with dimension 100×100 mm. As a heat source model, Goldak's double ellipsoid heat source model [14] was used. The heat distribution in a solid is described by the differential heat equation, which in the general case for the Cartesian coordinate system (x, y, z) has the form:

$$c\rho\frac{\partial T}{\partial t}=\frac{\partial}{\partial x}\left(\lambda\frac{\partial T}{\partial x}\right)+\frac{\partial}{\partial y}\left(\lambda\frac{\partial T}{\partial y}\right)+\frac{\partial}{\partial z}\left(\lambda\frac{\partial T}{\partial z}\right)+q, \quad (1)$$

where $c\rho$ — volumetric heat capacity of the material; λ — thermal conductivity; q — power distribution of a volumetric heat source.

Goldak's heat source model is built from two ellipsoids described with equations [14] for front part model q_f and rear part of model q_r:

$$q_f(x,y,z)=\frac{6\sqrt{3}f_fQ}{abc_f\pi\sqrt{\pi}}\exp\left(-3\left(\frac{x^2}{a^2}+\frac{y^2}{b^2}+\frac{z^2}{c_f^{\,2}}\right)\right); \quad (2)$$

$$q_r(x,y,z)=\frac{6\sqrt{3}f_rQ}{abc_r\pi\sqrt{\pi}}\exp\left(-3\left(\frac{x^2}{a^2}+\frac{y^2}{b^2}+\frac{z^2}{c_r^{\,2}}\right)\right). \quad (3)$$

The heat input rate $Q = \eta VI$ is defined by welding operational parameters current (I), voltage (V) and thermal efficiency (η), respectively. The factors f_f and f_r denote the fraction of the heat deposited in the front and rear quadrant respectively, which must satisfy the condition $f_f + f_r = 2$. The a, b_f, b_r and c are source constant parameters that define the size and shape of the ellipses, therefore the heat source distribution.

The cooling boundary conditions between the plate and surrounding environment by convection are calculated by the equation:

$$-\lambda\frac{\partial T}{\partial n}=h(T-T_0), \quad (4)$$

where T_0 (20 °C) is the room temperature and h (20 W·m^{-2}·K^{-1}) is the natural convective heat coefficient assumed.

Based on the solution of the heat equation by the finite element method, temperature fields of the calculation scheme were obtained. Calculation results of temperature fields for TIG welding process of DSS 2205 are given in Figures 2 and 3. The width of fusion zone ($T_{max} \geq$ 1450 °C) is 2.6 mm (at the bottom of the weld)-4.7 mm (at the top of the weld). Since the ferritic-austenitic transformation in duplex steels takes place in the temperature range from 1200 to

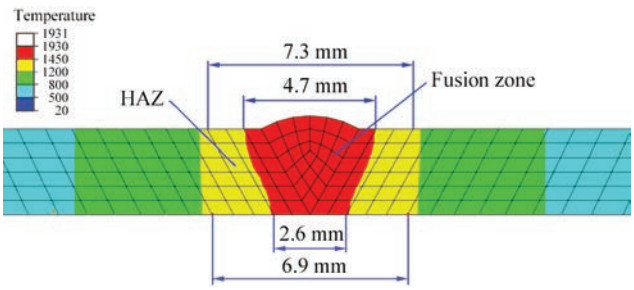

Figure 2. Dimension of the fusion zone and HAZ, mm

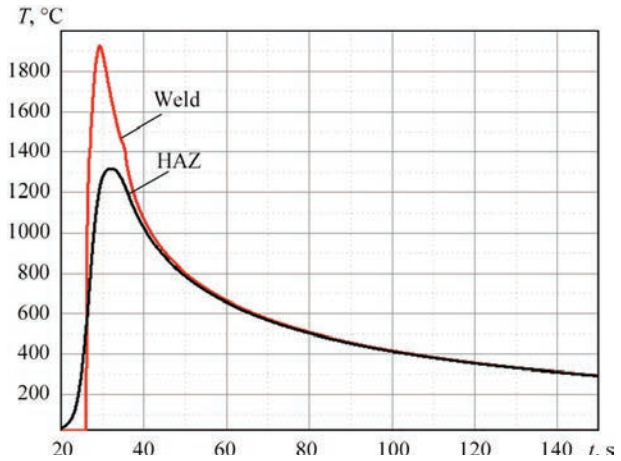

Figure 3. Characteristic thermal cycles in weld zone and HAZ

800 °C, the zone with the maximum heating temperature above 1200 °C was taken as the heat affected zone (HAZ). It`s depth in the base material is up to 1.3–2.15 mm (Figure 2).

An important characteristic during welding duplex steels is the cooling rate in the temperature range 1200–800 °C [15–17]. Since cooling is fast by the single pass welding, the obtained time $\Delta t_{1200/800}$ of the calculation model is equa 1 10–14s (Figure 3), the cooling rate $w_{1200/800}$ is from 28 to 40 °C/s. Comparison of cooling curve with TTT- and CCT-curve [18] shows, that due to fast speed cooling after welding (the cooling speed $w_{1200/800}$ = 28–40 °C/s >> 0.23 °C/s) the σ-phase (sigma phase) will not form. Sigma phase precipitation is possible during aging at high temperatures or in multi-pass welding [19, 20] due to low cooling rates.

The kinetics of the microstructure phase transformation during welding the DSS on the basis of literature data [17, 21] was modelled. Weldments of DSS with a Cr_{eq}/Ni_{eq} ratio above 1.95 (for steel S32205 Cr_{eq}/Ni_{eq} = 3.5) can be treated as a single-phase ferrite [22] when solidifying. The dissolution and precipitation kinetics of austenite in duplex stainless steels is followed by the Austin–Rickett type equation [17, 21]:

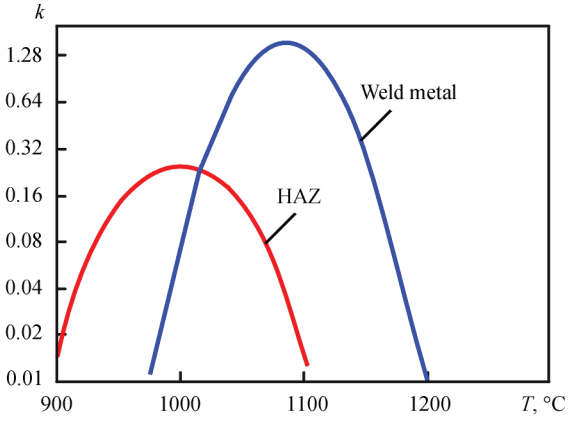

Figure 4. The precipitation kinetics constant $k(T)$ [21]

$$\frac{y}{1-y} = (kt)^n, \tag{5}$$

where y is the fraction transformed, k is the kinetics constant, t is the time and n is the time exponent.

The temperature dependency of dissolution rate $k(T)$ of austenite phase in DSSs is as follows [21]:

- for HAZ of standard DSSs

$$k(T) = \exp\left(-\frac{4.05 \cdot 10^4}{(T+273)} + 25.6\right); \tag{6}$$

- for weld metal of standard DSSs

$$k(T) = \exp\left(-\frac{5.82 \cdot 10^4}{(T+273)} + 37.4\right). \tag{7}$$

Temperature dependency of equi librium austenite phase fraction of standard DSS $F_{eq}(T)$ and precipitation parameters n, $k(T)$ were obtained from work [21] (Figure 4).

Since heating during the welding thermal cycle occurs without aging and cooling continuously with a variable cooling rate, the Austin-Rickett equa tion was accepted as modified equation taking into account the features of the welding thermal cycle. For this, the heating and cooling curve was divided into steps and the fraction of austenite was determined by the expression below [17]:

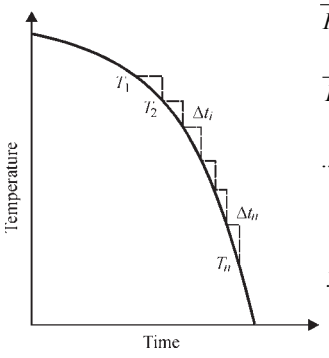

$$\frac{y}{Feq(T)-y} = [k(T)t]^n$$

$$\frac{y_j}{Feq(T_j)-y_j} = (k(T_1)+k(T_2)+\ldots$$

$$\ldots + k(T_j))^n \Delta t^n = \left[\Delta t \sum_{i=1}^{j} k(T_i)\right]^n$$

$$y_j = \frac{\left[\Delta t^n \sum_{i=1}^{j} k(T_i)^n Feq(T_i)\right]}{1+\left[\Delta t \sum_{i=1}^{j} k(T_i)\right]^n}. \tag{8}$$

The results of the microstructure composition and kinetics of phase transformation in the HAZ and weld metal shown in Figure 5 were obtained using Austin-Rickett equa tion (8) and precipitation parameters $k(T)$, n from work [21].

On the basis of equa tion (8) high content of austenite in weld metal and low content of austenite in HAZ was obtained. According to Figure 5 the phase composition in weld metal are 65 % austenite and 35 % ferrite, in the HAZ are 28 % austenite and 72 % ferrite. These data of microstructure composition (Figure 5) were used for the determining of the distribution of residual stresses after welding of DSS 2205.

Modelling of residual stresses, results and analysis

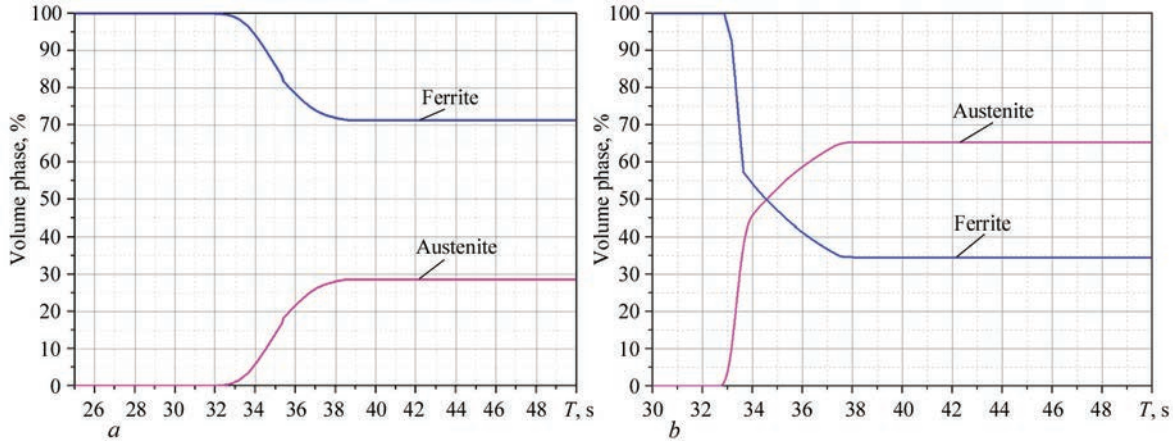

Figure 5. Kinetics of phase transformation during cooling of welding thermal cycle: *a* — point in the HAZ; *b* — point in the weld metal

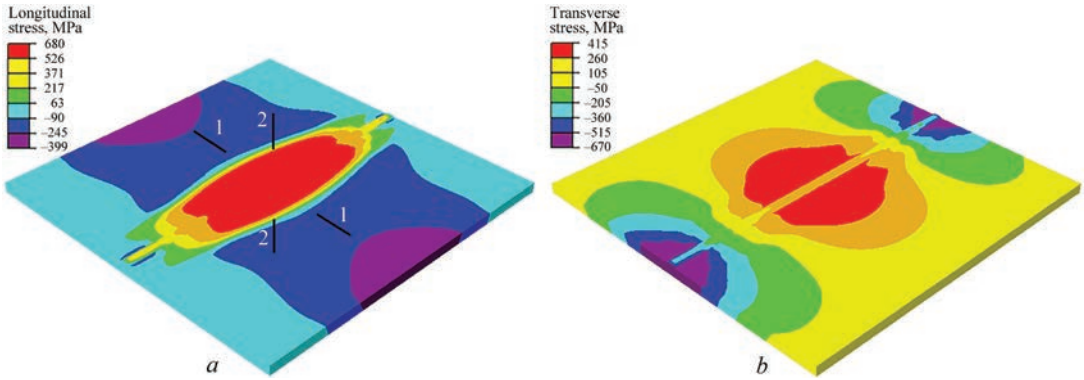

Figure 6. Residual stresses after welding and cooling without taking into account microstructural transformations: *a* — longitudinal stresses, MPa; *b* — transverse stresses, MPa

Phase transformations in steels can occur with significant volumetric changes, which mainly effects on the kinetics of the distribution of residual welding stresses and strains [23, 24].

The temperature and phase volume data presented in the previous section provided a framework to comparatively study the residual stresses with/without taking into account of the microstructural transformations, typical results are shown in Figures 6, 7. Figure 6 is a plot of residual stress without taking into account of the phase changes, while Figure 7 is result incorporated the microstructural transformations in the model. A significant difference could be observed in the distribution pattern and magnitudes of the residual stresses.

Figure 8 compares the profiles of residual stresses along cross-section 1 (transversely to the weld) for model without phase transformations and model taking into account of phase transformations. It clearly shows that residual stresses distribution from these two approaches is different for both the longitudinal and the transverse stresses, with the latter exhibit more significant differences. With a lower austenite content/higher ferrite content in the heat affected zone, a decrease in tensile longitudinal residual stresses is observed.

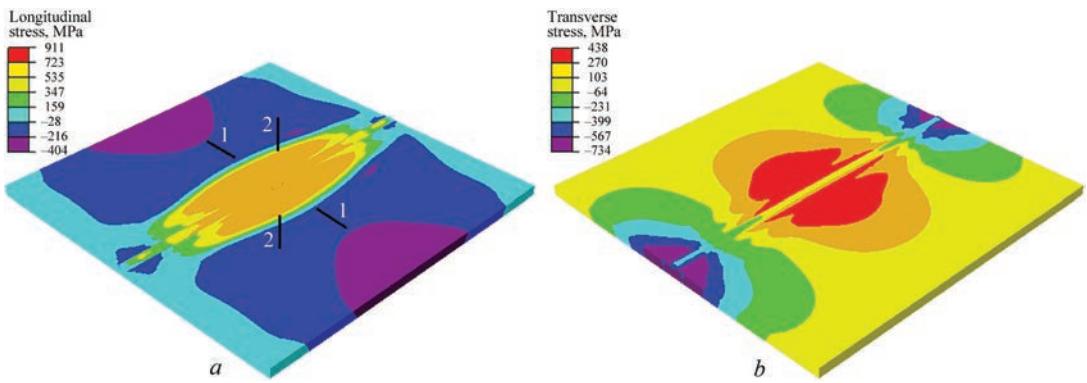

Figure 7. Residual stresses after welding and cooling taking into account the kinetics of austenitic transformation: *a* — longitudinal stresses, MPa; *b* — transverse stresses, MPa

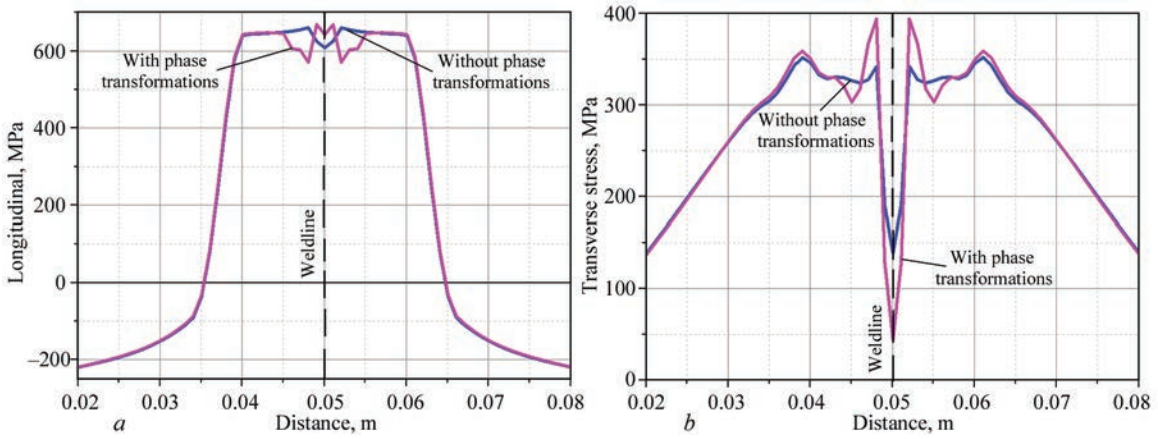

Figure 8. Residual stresses distribution through cross-section 1: *a* — longitudinal stresses; *b* — transverse stresses

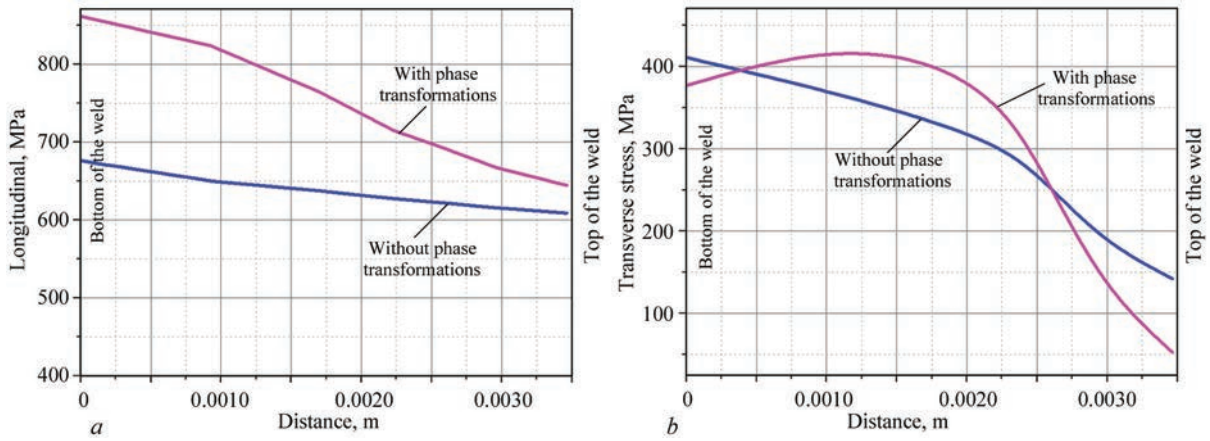

Figure 9. Residual stresses distribution through cross-section 2: *a* – longitudinal stresses; *b* – transverse stresses

Figure 9 compares the distributions of simulated residual stresses along cross-section 2 (through thickness of the weld) for model without phase transformations and model taking into account phase transformations. The longitudinal stresses from both modelling approaches show a gradual reducing trend with the distance (from root to top of the weld) before the difference becoming less significant. In the transverse stress data, the trend in the residual stresses is different between these two modelling approaches. The stresses level gradually decreases from root to top of the weld for the model without considering the phase transformation, while the data from the model considering the phase transformations show an increase in the stress first followed by a decrease trend at the top of the weld.

Compared to the results without phase transformations, the difference in the magnitudes of the residual stresses is up to 50–100 MPa in cross-section 1 and up to 90–185 MPa in cross-section 2. In future works, systematic data with different welding conditions of samples with different dimensions/constraints will be further developed, the effect of the residual stresses on the strength, toughness and corrosion will be studied.

Conclusions

1. In the present study TIG single-pass welding process of duplex stainless steel S32205 taking into account of microstructural transformations was simulated. The obtained cooling rate in the temperature range 1200–800 °C (time $\Delta t_{1200/800}$) is equal 10–14 s.

2. Using calculating method on the basis of the Austin-Rickett equation, the predicted data of obtained austenite content 65 % — in the weld and 28 % — in the HAZ.

3. The microstructural transformations showed an influence on the distribution of residual stresses after welding of DSS. In comparison with residual stresses without phase transformations, a higher value of longitudinal residual stresses was obtained in the weld with high amount of austenite. In the case of a lower austenite content (in the HAZ) accounting of phase transformations leads to a decrease in the tensile longitudinal residual stresses value and an increase of transverse tensile residual stresses value.

Acknowledgments. *The present study was financially supported by EU Horizon 2020 MSCA-RISE Project (i-Weld) No. 823752.*

1. (2014) Practical guidelines for the fabrication of duplex stainless steels. *International Molybdenum Association* (IMOA); 3nd Ed.
2. Ammann, T. (2007) Arc welding of duplex steels in a shielding gas environment. *Svetsaren, the ESAB Welding and Cutting Journal*, 62(**1**), 41–45 [in Russian]. ?????
3. (2019) Duplex stainless steels welding guidelines. *Industeel Arcelor Mittal*, June.
4. (2011) *API Technical Report 938C: Use of Duplex Stainless Steels in the Oil Refining Industry*, Second Ed.
5. Pramanik, A., Littlefair, G., Basak, A.K. (2015) Weldability of duplex stainless steel. *Materials and Manufacturing Processes*, 30(**9**), 1053–1068; DOI: 10.1080/10426914.2015.1019126
6. Vahid Hosseini (2018) *Super duplex stainless steels — microstructure and properties of physically simulated base and weld metal*: PhD Thesis Production Technology, 24. University West, Sweden.
7. Kim, Yoon-Jun (2004) *Phase transformations in cast duplex stainless steels.* Other Information: TH: Thesis (Ph.D.); Submitted to Iowa State Univ., Ames, IA (US); PBD: 19 Dec.
8. Brytan, Z., Niagaj, J., Pakieła, W., Bonek, M. (2015) FEM modeling of lean duplex stainless steel welding. *J. of Achievements in Materials and Manufacturing Engin.*, 70(**1**), 36–44.
9. Gideon, B., Ward, L., Carr, D.G., Muransky, O. (2008) Duplex stainless steel welds: residual stress determination, magnetic force microscopy and susceptibility to intergranular corrosion. In: *Proc. of 6th European Stainless Steels Conf., Helsinki, Finland, 10–13 June 2008*, F-2P, 629–636.
10. Giętka, T., Ciechacki, K., Kik, T. (2016) Numerical simulation of duplex steel multipass welding. *Archives of Metallurgy and Materials*, 61(**4**), 1975–1984, December.
11. Floreka, A., Křížb, A., Vilcsekc, I. (2019) Numerical modelling of welding of duplex steel. In: *AIP Conf. Proceedings* 2189, 020006.
12. Tae-Hwan Um, Chin-Hyung Lee, Kyong-Ho Chang, Vuong Nguyen Van Do (2018) Features of residual stresses in duplex stainless steel butt welds. *IOP Conference Series Earth and Environmental Science,* 143(**1**):012030
13. Leffler, B. (2013) *Stainless steels and their properties.* http://www.hazmetal.com/f/kutu/1236776229.pdf
14. Goldak, J., Chakravart, A., Bibby, M. (1984) A new finite element model for welding heat sources. *Metallurgical Transact. B, Process Metallurgy*, 15(**2**), 299–305. http://dx.doi.org/10.1007/BF02667333.
15. Toshio Kuroda, Kenji Ikeuchi, Yoshihiko Kitagawa (2004) Microstructure control for joining advanced stainless steel. In: *Proc. of the Intern. Symp. on Novel Materials Processing by Advanced Electromagnetic Energy Sources (March 1922, 2004, Osaka, Japan)*, 419–422.
16. Varbai, B., Adonyi, Y., Baumer, R. et al. (2019) Weldability of duplex stainless steels — thermal cycle and nitrogen effects: Duplex stainless steel weld microstructures were investigated as a function of weld thermal cycles and shielding gas nitrogen content. *Welding J.*, **98**, 78–87.
17. Koichi Yasuda, Robert N. Gunn, Trevor G. Gooch (2002) Prediction of Austenite Phase Fraction in Duplex Stainless Steel Weld Metals. *Qarterly J. of the Japan Welding Society*, 20(**1**), 68–77.
18. Sieurin, H., Sandstrom, R. (2007) Sigma phase precipitation in duplex stainless steel 2205. *Materials Sci. and Engin. A*, **444**, 271–276.
19. Nishimoto, K., Saida, K., Katsuyama, O. (2006) Prediction of sigma phase precipitation in super duplex stainless steel weldments. *Weld World*, **50**, 13–28. https://doi.org/10.1007/BF03263429
20. Makhnenko, V.I., Kozlitina, S.S., Dzyubak, L.I. (2011) Forecasting the content of σ-phase in the HAZ of welded joints of duplex steels in arc welding. *The Paton Welding J.*, **6**, 6–8.
21. Ogura T., Matsumura T., Yu L. et al. (2018) Numerical simulation of ferrite/austenite phase fraction in multipass welds of duplex stainless steels. Mathematical modelling of weld phenomena 12. In: *Proc. of Intern. Sem. Numerical Analysis of Weldability, Graz, Austria*. DOI 10.3217/978-3-85125-615-4-07
22. Ghusoon Ridha Mohammed, Mahadzir Ishak, Syarifah N. Aqida, Hassan A. Abdulhadi (2017) Effects of heat input on microstructure, corrosion and mechanical characteristics of welded austenitic and duplex stainless steels: A *Review. Metals — Open Access Metallurgy J.*, 7(**2**), 39.
23. Makhnenko, V.I., Velikoivanenko, E.A., Pochinok, V.E. et al. (1999) Numerical methods for the prediction of welding stress and distortions. *Welding and Surfacing Reviews*, 13(**1**).
24. Yuriev, S.F. (1950) *Specific volume of phases in the martensitic transformation of austenite*. Moscow, Metallurgizdat [in Russian].

Received 08.12.2020